HHS Public Access

Author manuscript

J Aerosol Sci. Author manuscript; available in PMC 2015 July 08.

Published in final edited form as:

J Aerosol Sci. 2013 July ; 61: 50–59.

Development of a new test system to determine penetration of multi-walled carbon nanotubes through filtering facepiece respirators

Evanly Vo* and **Ziqing Zhuang**

National Institute for Occupational Safety and Health, National Personal Protective Technology Laboratory, 626 Cochrans Mill Road, Pittsburgh, PA 15236, USA

Abstract

Carbon nanotubes (CNTs) are currently used in numerous industrial and biomedical applications. Recent studies suggest that workers may be at risk of adverse health effects if they are exposed to CNTs. A National Institute for Occupational Safety and Health (NIOSH) survey of the carbonaceous nanomaterial industry found that 77% of the companies used respiratory protection. Elastomeric half-mask respirators and filtering facepiece respirators (FFRs) are commonly used. Although numerous respirator filtration studies have been done with surrogate engineered nanoparticles, such as sodium chloride, penetration data from engineered nanoparticles such as CNTs are lacking. The aims of this study were to develop a new CNT aerosol respirator testing system and to determine multi-walled CNT (MWCNT) penetration through FFRs.

A custom-designed CNT aerosol respirator testing system (CNT-ARTS) was developed which was capable of producing a sufficient amount of airborne MWCNTs for testing of high efficiency FFRs. The size distribution of airborne MWCNTs was 20–10,000 nm, with 99% of the particles between 25 and 2840 nm. The count median diameter (CMD) was 209 nm with a geometric standard deviation (GSD) of 1.98. This particle size range is similar to those found in some work environments (particles ≤6000 nm). The penetration of MWCNTs through six tested FFR models at two constant flow rates of 30 and 85 LPM was determined. Penetration at 85 LPM (0.58–2.04% for N95, 0.15–0.32% for N99, and 0.007–0.009% for P100 FFRs) was greater compared with the values at 30 LPM (0.28–1.79% for N95, 0.10–0.24% for N99, and 0.005–0.006% for P100 FFRs). The most penetrating particle size through all six tested FFR models was found to be in the range of 25–130 nm and 35–200 nm for the 30-LPM and 85-LPM flow rates, respectively.

Keywords

Multi-walled carbon nanotubes; Carbon nanotube aerosol respirator testing system; Airborne carbon nanotubes; Filtering facepiece respirators; Filtration

*Corresponding author. Tel.: +1 412 386 5201; fax: +1 412 386 5250. Eav8@cdc.gov (E. Vo).

Disclaimer

The findings and conclusions in this manuscript are those of the authors and do not necessarily represent the views of the National Institute for Occupational Safety and Health (NIOSH). Mention of company names or products does not constitute endorsement by NIOSH.

1. Introduction

Carbon nanotubes (CNTs) are currently used in numerous industrial and biomedical applications, including electron field emitters, conductive plastics, semiconductor devices (Wang et al., 2011a, 2011b; Endo et al., 2008), chemical sensors and catalysts (McKinney et al., 2009), biosensors, and medical devices (Endo et al., 2008; Chakravarty et al., 2008). The concern about worker exposure to CNTs arises from results of animal toxicological studies. Several studies in rodents have shown: (1) acute pulmonary inflammation and interstitial fibrosis observed in CNT-exposed animals in subchronic studies (Shvedova et al., 2008; Porter et al., 2010) and (2) an equal or greater potency of CNTs compared to other inhaled particles known to be hazardous to exposed workers (crystalline silica and asbestos) in causing adverse lung effects (Shvedova et al., 2005; Muller et al., 2005). Animal toxicological evidence suggests that the potential for a wide range of human health effects which could result from exposure to CNTs (NIOSH-161A, 2010; Poland et al., 2008).

The number of carbon layers in nanotubes varies from one layer in single-walled CNTs (SWCNTs) to many layers in multi-walled CNTs (MWCNTs). Although CNTs come in a variety of types, they all tend to form large agglomerates (bulk powder) due to their fibrous geometry and van der Walls forces; therefore, dispersion of airborne CNTs in a respirable size plays a significant role in CNT studies. Researchers have developed different methods to disperse CNTs, including mechanical agitation methods (Maynard et al., 2007; Mitchell et al., 2007), acoustic methods (Baron et al., 2008; McKinney et al., 2009), atomizers (Seto et al., 2010), and electrosprays (Ku & Kulkarni, 2009; Wang et al., 2011b). However, questions have arisen as: (1) whether the energy associated with these CNT separation methods change the physical properties of CNTs compared with those found in the work environment, (2) whether the atomizer and electrospray dispersion methods produce uniform airborne CNTs when dealing with the low-solubility CNTs, or (3) whether these dispersion methods are able to produce a sufficient amount of airborne CNTs with a controlled degree of agglomeration for testing of high efficiency filtering facepiece respirators (FFRs).

It has been suggested that workers may be at risk for exposure to CNT particles during the manufacture, handling, and cleanup of CNT materials (Mitchell et al., 2007; Porter et al., 2010). Recently, a NIOSH survey of the carbonaceous nanomaterial industry found that 77% of the companies used some respiratory protection (Dahm et al., 2011). Elastomeric half-mask respirators and FFRs are commonly used (Dahm et al., 2011). The NIOSH Current Intelligence Bulletin recommends workers to use and select respirators when working with nanoparticles (NIOSH-161A, 2010).

Although numerous respirator filtration studies have been done with surrogate engineered nanoparticles, such as sodium chloride, reports on the penetration of airborne CNTs through FFRs are lacking. These previous studies were used solvents as aerosol generator fluids (suspension solutions), targeted toward generating spherical particles, and measured for particles in the range of 100–400 nm mobility diameters (Wilkes, 2002; Rengasamy et al., 2009). Thus, development of a new aerosol respirator testing system to determine elongated-shape CNT penetration through FFRs or other respirator filters and to support the current NIOSH respirator recommendations is needed.

The aim of this study was to develop a new test system to measure the filtration performance of FFRs using airborne MWCNTs. The new system was designed to achieve four specific research objectives: (1) to be capable of generating airborne MWCNT particles continuously and uniformly, with a respirable MWCNT aerosol similar in size to those found in the workplace (particle size ≤6 μm; Han et al., 2008; McKinney et al., 2009), (2) to produce a sufficient amount of airborne MWCNTs for testing of high efficiency FFRs [a P100-FFR penetration level is ≤0.03% (NIOSH-42 Part 84, 1995), so a minimum MWCNT concentration required for P100-FFR penetration test is $\geq 3 \times 10^4$ particles/cm^3], (3) to be able to maintain a stable desired concentration during a test period, and (4) to be capable of performing MWCNT filter penetration tests.

2. Materials and methods

2.1. Equipment and supplies

2.1.1. CNT aerosol respirator testing system—A custom-designed CNT aerosol respirator testing system (CNT-ARTS) consists of a CNT aerosol generation system, a particle detector system, and a penetration measurement system (Fig. 1). The CNT aerosol generation system consists of a 6-jet Collison nebulizer (BGI, Waltham, MA), a stir plate, a micro-stir bar (SBM-2003-MIC; 20-mm length and 3-mm diameter), a respirable cyclone (Model: GK4.162; BGI), a diffusion dryer, a Kr-85 aerosol neutralizer (Model 3054, TSI Inc., Shoreview, MN), and a Condensation Particle Counter (CPC, model 3776; TSI) used to monitor the output CNT concentration. A compressed air supply for the generator was filtered with a high efficiency particulate air (HEPA) filter. The particle detector system consists of a Scanning Mobility Particle Sizer (SMPS; model 3080; TSI; detection range: 0.01–1 μm), including a CPC (model 3776) and an Aerodynamic Particle Sizer (APS, Model 3321, TSI; detection range: 0.5–20 μm). The penetration measurement system consists of an exposure chamber system, a leakage test system, and a constant air flow system. The exposure chamber system consists of a 48-L acrylic exposure chamber (Vandiver Enterprises, Zelienople, PA), a humidity/temperature sensor, a circulation fan, a humidity/temperature controller, and a 1-cm diameter exhaust port (one-way airflow valve; Model #123, TSI) to remove excess air from the chamber during particle generation and sampling. The width, depth, and height of the exposure chamber is 36 cm × 36 cm × 37 cm, respectively so that a head form with an FFR could be placed inside the chamber for the penetration test and be easily disassembled for cleaning. Because of CNT aerosol safety concerns, the exposure chamber was set up inside a secondary acrylic containment chamber (100 cm × 100 cm × 80 cm as width, depth, and height, respectively) which also has a 9-cm diameter exhaust port, containing a HEPA filter and an internal fan to direct air flow (Electro-Tech System, Glenside, PA). The leakage test system consists of a plaster-material head form and Series 1101 breathing simulator (Hans Rudolph). The constant air flow system consists of a head form with an FFR, a mass flow meter (Model #4045, TSI), a HEPA filter, and an in-house vacuum with an air regulator to control the air flow rate.

2.1.2. MWCNT samples—The MWCNT bulk materials used in this study were obtained from the Nanostructured & Amorphous Materials Inc. (MWNT-1227YJS, lot 1227–041709; Houston, TX) and used without further purification. The average width of the stock

MWCNTs is between 30 and 80 nm, while the average length is between 0.5 and 2 μm. MWCNTs were selected for this study based on their worldwide high-volume production with about 300 t/year (WTEC, 2007) and the worker exposure concern regarding the asbestos-like pathogenicity of MWCNTs (Poland et al., 2008).

2.1.3. Respirators—Two models of each N95, N99, and P100 series (total six tested FFR models) were selected randomly from among those models tested previously (Vo & Shaffer, 2012) in our laboratory (Table 1). These models are NIOSH-approved FFR models and are commonly used by workers in the carbonaceous nanomaterial industry (Dahm et al., 2011). These FFRs had multilayer structure, and the main layers of these FFRs were composed of polypropylene fibers with electrical charge; however, each FFR model has different characteristics, such as number of layers, thickness, and different hydrophilic and hydrophobic fiber materials.

2.2. Generation of airborne MWCNT in CNT-ARTS

In order to achieve the study objectives of generating airborne-form MWCNTs in the respirable-size, producing a sufficient amount of airborne MWCNTs for testing of high efficiency FFRs, and maintaining a stable desired concentration during a test period, a new CNT aerosol generation system was designed and set up as illustrated in Fig. 2. A nebulizer coupled to a micro-stir bar/stir plate was used to generate airborne MWCNTs. The micro-stir bar was used to excite MWCNT samples and disperse them from bulk-powder materials without using any solvents to disperse the bulk MWCNTs in the nebulizer. The 7-LPM air to nebulizer was used to carry small MWCNT particles out of the nebulizer cylinder, while larger particles tended to stay in the lower portion of the cylinder until they were dispersed. A cyclone was used to remove larger particles to ensure all airborne MWCNTs produced were in the respirable-sized range. The output concentration of the airborne MWCNTs was monitored using a CPC and controlled to maintain a stable desired concentration during a test period by adjusting the speed level of the stir bar.

During generator operation, 1.0 g of bulk MWCNTs and a small stir bar were placed inside the nebulizer cylinder. After the head form with the FFR sealed to it was set up, the chamber was closed and internal fans were turned on. Then, compressed air valves were opened and particles were generated. The airflow to the nebulizer was set to 7 LPM and the stir plate was operated at a low speed to gently disperse the CNTs. The MWCNT particles passed through a cyclone to establish the size cut of particles ≥10 μm before they were directly mixed with clean dry air to reach a final designated MWCNT concentration. Then the airborne MWCNTs passed through diffusion dryer to enhance the removal of liquid vapors. Before entering the 48-L exposure chamber, the airborne MWCNTs passed through a Kr-85 neutralizer. MWCNT particles were continuously generated and passed into the chamber, while the chamber conditions were maintained at 23 °C and 35% RH.

2.3. Characterization of airborne MWCNT in CNT-ARTS

2.3.1. Output MWCNT concentration during a test period—To investigate a stable concentration, the CPC with a controlled flow rate of 1.5 LPM was used to measure the MWCNT concentration in the exposure chamber for a 30-min test period. Normally, the

CPC was used to monitor the output MWCNT concentration in the chamber during particle generation.

2.3.2. MWCNT uniformity in the exposure chamber—The APS (Fig. 1, 5A) and SMPS, including the CPC (Fig. 1, 5B), were used to investigate the MWCNT uniformity in the chamber at 9 different chamber locations designated as: back-left top (BLT), front-left top (FLT), back-right top (BRT), front-right top (FRT), center (C), back-left bottom (BLB), front-left bottom (FLB), back-right bottom (BRB), and front-right bottom (FRB). The combination of the SMPS and APS data into a single size distribution (20–10,000 nm) was performed according to the method of Khlystov et al. (2004) by calculating the ratio of the overlapping size range between 600 and 900 nm. This method allows measuring the concentration and size distribution of airborne MWCNT particles in a wide size range from 20 to 10,000 nm into a single plot, and was used for all APS and SMPS data set from this study.

2.3.3. Characterization of upstream and downstream airborne MWCNTs—Upstream airborne MWCNTs were characterized using the same procedure as described in the “MWCNT uniformity in the exposure chamber” section. The concentration and size distribution of airborne MWCNTs outside each tested FFR (near the center) were used for this test and designated as upstream particles.

The concentration and size distribution of airborne MWCNTs inside each tested FFR were measured for each FFR model. The MWCNT particles inside each tested FFR were designated as downstream particles.

2.4. FFR penetration against airborne MWCNT particles

2.4.1. Leakage test—Before each penetration experiment, a leakage test was conducted by using a breathing system (Fig. 1, 3B and 3C). An FFR was sealed with silicone to the face of the head form so that no leakage occurred between the face and the inner filter surfaces. In addition, each N99 and P100 FFR, containing an exhalation valve, was also sealed with silicone to avoid any leakages from the exhalation valve (both N95 FFR models did not have an exhalation valve). The head form was connected to a breathing simulator using a plastic breathing tube. Then, the silicone sealant surface was covered by a bubble-producing liquid, and a leakage test was conducted at a 30-LPM (1.2 L/stroke × 25 strokes/min) waveform to determine if the exhaled air caused bubble formation due to leakages. If any leaks were detected, additional silicone was applied to the seal and the leak check was repeated.

2.4.2. FFR penetration—Penetration for sealed FFRs was measured using the SMPS and APS. The MWCNT penetration through the FFR was determined based on the downstream and upstream concentrations recorded in each SMPS-APS experimental data set. The penetration experiments were carried out using the penetration measurement system at two constant flow rates for each model: 30 LPM (which simulates inhalation at a normal work rate; Clayton et al., 2002) and 85 LPM (which simulates inhalation at a heavy work rate; Clayton et al., 2002).

The penetration outputs for each model were reported as: (1) penetration as a function of individual particle size and (2) total penetration of all particle sizes. Penetration (P in %) as a function of individual particle size was calculated as a ratio of the downstream and upstream concentrations:

$$P=(C_{\text{down}}/C_{\text{up}}) \times 100 \quad (1)$$

where C_{down} is the downstream CNT concentration (mean particles that penetrated the FFR of each model) at each particle size; C_{up} is the upstream CNT concentration at each particle size.

The total penetration (P_t in %) of all particle sizes provided particle penetration across the full size range measured, and was calculated as:

$$P_t=(\sum C_{\text{down}}/\sum C_{\text{up}}) \times 100 \quad (2)$$

where ΣC_{down} is the total downstream MWCNT concentrations and ΣC_{up} is the total upstream MWCNTs.

2.5. Data analysis

All tests from this study were replicated three times. The mean, standard deviation, the coefficient of variation (CV) values, and normal data distribution were calculated using Microsoft Excel 2010 software (Microsoft Corporation, Redmond, WA). *P*-values of <0.05 were considered significant. To compare the percent penetration of MWCNT particles through each FFR model, obtained from both the constant flow rates of 30 and 85 LPM, paired *t*-tests with two-tailed distribution were run, also using Microsoft Excel 2010.

3. Results

3.1. Characterization of airborne MWCNT in CNT-ARTS

The average MWCNT concentrations in the “output MWCNT concentration during a test period” experiment were found to be 2.35×10^5 ($\pm 8.01 \times 10^3$) particles/cm^3 (n=3; Fig. 3). The results show that the CNT-ARTS was capable of maintaining a stable MWCNT concentration during a test period. The CNT aerosol generator was able to produce a sufficient amount of airborne MWCNTs (up to 2.78×10^5 particles/cm^3; Figs. 4 and 5) for testing of high efficiency FFRs.

The average size distributions and concentrations of airborne MWCNTs at different chamber locations were determined and are shown in Fig. 4. The average concentration of airborne MWCNT particles ranged from 2.52 to 2.78×10^5 particles/cm^3 (n=3). All CVs at different chamber locations were found to be ≤1.93%. The results indicate that the MWCNT concentrations and size distributions were relatively uniform throughout the chamber.

The size distribution and concentration of upstream airborne MWCNTs were characterized using the SMPS and APS. The size distribution was in the range of 20–10,000 nm, with 99% of particles centered between 25 and 2840 nm (Fig. 5). The count median diameter (CMD) was 209 nm with a geometric standard deviation (GSD) of 1.98 and a mode of 260 nm.

The size distribution of downstream MWCNTs at the constant flow rate of 30 LPM was determined for each FFR model, ranging from 20 to 4300 nm, with 99% of particles centered between 25 and 1486 nm for all FFR models (Fig. 5). The CMD was found to be in the range of 110–180 nm with GSD in the range of 1.40–1.89 for all six tested FFR models.

3.2. MWCNT penetration

Percent penetration values for the six tested FFR models at constant flow rates of 30 and 85 LPM as a function of individual particle size are shown in Fig. 6. For the 30 LPM, average percent penetrations were highest for the N95 (0.28–1.79%), followed by N99 FFRs (0.10–0.24%) and P100 (0.005–0.006%). The paired *t*-tests ran for Gerson N95 and North N95 models revealed *P*-values of 0.002 and 0.001 for the flow rates of 30 and 85 LPM, respectively. This indicates that penetrations were significantly different between Gerson N95 and North N95 models; however, penetrations were not significantly different between Moldex N99 and Willson N99 ($P \geq 0.06$) or 3M P100 and Sperian P100 models ($P \geq 0.34$). Fig. 6 also shows that the penetration of the N95 North approached the performance of the Moldex N99 model over particle sizes with *P*-values of 0.79 and 0.33 for the flow rates of 30 and 85 LPM, respectively. In general, different FFR models yielded different MWCNT penetrations. Mean particle penetration at 85 LPM (0.58–2.04% for N95, 0.15–0.32% for N99, and 0.007–0.009% for P100 FFRs) was greater compared with the values at 30 LPM (0.28–1.79% for N95, 0.10–0.24% for N99, and 0.005–0.006% for P100 FFRs) for all six FFR models (Fig. 6). Paired *t*-tests ran for each N95 model compared penetration at flow rates of 30 and 85 LPM indicate a significant difference between the two flow rates for a given model: $P=0.005$ for Gerson N95 and $P=0.0121$ for North N95. However, penetrations were not significantly different between the two flow rates for each N99 or P100 model (all *P*-values ≥0.06). The most penetrating particle size (MPPS) through all six FFR models at the flow rate of 30 LPM was found to be in the range of 25–130 nm (30–130, 30–100, 30–90, 25–130, 38–100, and 40–120 nm for Gerson N95, North N95, Moldex N99, Willson N99, 3M P100, and Sperian P100, respectively; Fig. 6), while the MPPS at 85 LPM was found to be in the range of 35–200 nm (45–200, 40–190, 35–135, 40–190, 48–185, and 50–185 nm for Gerson N95, North N95, Moldex N99, Willson N99, 3M P100, and Sperian P100, respectively; Fig. 6).

The total penetration of all particle sizes at constant flow rates of 30 and 85 LPM are shown in Fig. 7. The results indicate that the penetrations at 85 LPM were greater compared with the values at 30 LPM for all FFR models. Comparison of the results between two methods of calculating penetration indicated that the total penetration was consistently higher than those in the penetration as a function of individual particle size for all FFR models.

4. Discussion

The CNT-ARTS was capable of generating airborne MWCNT particles continuously and uniformly in a sufficient amount for testing of high efficiency FFRs. With a cyclone and a low air flow rate to nebulizer, the CNT aerosol generator was able to produce airborne MWCNTs in a respirable range similar in size to those found in work environments (particle size ≤6000 nm; Maynard et al., 2004; McKinney et al., 2009). These results indicate that the

CNT-ARTS was capable of generating airborne MWCNT particles with a controlled degree of agglomeration.

The CNT-ARTS was also capable of producing a stable desired MWCNT concentration during a test period by adjusting the speed level of the stir bar. MWCNT concentration could be controlled by other test parameters, such as varying the air-flow rate to the nebulizer or changing the volume of dilution air; however, to keep constant exposure-chamber conditions (temperature and RH) and to minimize the amount of MWCNTs used, the output MWCNT concentration was only controlled by adjusting the speed level of the stir bar.

Comparison of the results at different chamber locations indicated that the new test system not only generated a designated particle size, but also generated similar particle counts throughout the chamber. The use of the CNT-ARTS also allowed us to solve three major problems of dispersing CNTs: (1) the low energy associated with this CNT separation method (using stir plate/stir bar) did not change the physical properties of CNTs because the output particle sizes were similar to those found in the work environments (particle size ≤6000 nm), (2) using powder-form CNTs (no solvents were used as generator fluids) allowed us to produce uniform CNT particles without dealing with the low-solubility CNTs, and (3) the new test system was able to produce a sufficient amount of airborne CNTs with a controlled degree of agglomeration for testing of high efficiency FFRs.

The size difference between upstream (20–10,000 nm) and downstream (20–4300 nm) MWCNTs indicated that airborne MWCNTs with the particle size >4300 nm were completely captured on the fibers of the FFRs for all six FFR models. Only MWCNTs with a particle size ≤4300 nm were able to penetrate through the FFR. In general, mechanisms for MWCNT capture included diffusion, interception, electrostatic attraction and inertial impaction, because gravitational settling is negligible for nanoparticles (Seto et al., 2010). Although the capture efficiency of MWCNT particles with elongated shapes (ratio of length to diameter >3:1) due to diffusion is similar to the capture efficiency of spherical particles such as sodium chloride with the same electrical mobility size (Kim et al., 2009), the capture efficiency of the elongated MWCNTs due to interception and inertial impaction would be dominant mechanisms for the MWCNTs with their curling/bending shape (Wang & Pui, 2009; Wang et al., 2011a, 2011b) and their long rotation time (aspect ratios between the geometric length and the diameter of MWCNTs are in the range of 6–67).

The results of the penetration as a function of individual particle size at flow rates of 30 and 85 LPM show that different FFR models yielded different MWCNT penetrations, with larger penetrations observed for each model at the higher flow rate. The penetration data also show that the particle size increased with increasing flow rate. Average percent penetrations for both 30-LPM and 85-LPM experiments had a similar trend in the penetration and were highest for the N95 FFRs, followed by N99 and P100 FFRs. The filter properties (polypropylene fibers and electrical charges), numbers of filter layers, and total filter thickness would contribute to this penetration trend among the three different FFR series: N95, N99, and P100. For different FFR models within each FFR series, the results show that penetrations were significantly different between Gerson N95 (1.79%) and North

N95 (0.28%) models. A possible explanation for the different penetrations is that the North N95 FFR model has a hydrophobic outer layer, while Gerson N95 model has a hydrophilic outer layer. However, penetrations were not significantly different between Moldex N99 and Willson N99 or 3M P100 and Sperian P100 models. A possible explanation for the similar penetrations is that both Moldex N99 and Willson N99 or 3M P100 and Sperian P100 models have the same number of filter layers and hydrophilic/hydrophobic layer characteristics.

The penetration data also show that the particle size increased with increasing flow rate. Some previous studies on mechanical filters found that the MPPS was in the size range of 100–400 nm for inert nanoparticles, such as sodium chloride aerosol (Howard, 2003). However, we found that the MPPS for MWCNTs penetrated through the FFRs, which have electret filters, the most common type of filter used in respirators on the market today, was in the range of 25–130 nm and 35–200 nm for the 30-LPM and 85-LPM flow rates, respectively. The main reason for the differences is that the particle deposition on mechanical filters occurs because of diffusion, direct interception, and inertial impaction, while the electret filters are composed of charged fibers. This property leads to a considerable shift of the maximum penetration toward smaller particles because the additional polarization force has a great importance in the process of the particle deposition on fibers. Similar MPPS results were reported by other NIOSH researchers who found that the MPPS range for electret filters is between 30 and 100 nm for inert nanoparticles such as sodium chloride aerosol (Rengasamy et al., 2007, 2009, 2011). The reason NIOSH tests respirators using inert nanoparticles such as sodium chloride is that the filtration performance would likely be lower for spherical particles than for elongated CNTs. The results of this paper support continued use of the current NIOSH respirator recommendations for protection against nanoparticles.

Comparison of the results between the two methods of calculating penetration indicated that the total penetration was consistently higher than those in the penetration as a function of individual particle size for all FFR models. The results from this study also indicate that the P100-class respirators had higher levels of laboratory filtration performance compared to N95-class respirators for both methods of calculating penetration.

5. Study limitations

In this study, the FFRs were sealed to the face of the head form and exhalation valves were sealed, so the efficiency determined during experiments was defined as the efficiency of the FFR filter material. The actual field-measured penetration may be higher if there are some leakages between the wearer’s face and the FFR or any leakages from the FFR exhalation valve. It must also be noted that in this study only limited FFR models were tested and that other models may perform better or worse than those selected.

6. Conclusions

A CNT aerosol respirator testing system was successfully designed, constructed, and used to perform FFR penetration test. This system was capable of (1) generating airborne MWCNT particles continuously, with a respirable MWCNT aerosol similar in size to those found in

the workplace, (2) producing a sufficient amount of airborne MWCNTs for testing of high efficiency FFRs, (3) maintaining a stable desired concentration during a test period, and (4) performing MWCNT penetration tests. This study found that penetration of MWCNT at 85 LPM was greater compared with the values at 30 LPM. The most penetrating particle size through all six tested FFR models was found to be in the range of 25–130 nm and 35–200 nm for the 30-LPM and 85-LPM flow rates, respectively. Based on these promising results, CNT-ARTS could find utility in measuring filter penetration for other types of powder-form engineered nanoparticles (e.g., SWCNT, carbon black, metal oxides, etc.).

Acknowledgments

This study was partially supported by the NIOSH Nanotechnology Research Center (NTRC). The authors thank Dr. Samy Rengasamy, Dr. William P. King, Dr. Ron Shaffer (NIOSH/NPPTL, Pittsburgh, PA), and Dr. Peter A. Jaques (URS Corp., Pittsburgh, PA), for their valuable assistance in the preparation of the manuscript.

References

Baron PA, Deye GJ, Chen BT, Schwegler-Berry DE, Shvedova AA, Castranova V. Aerosolization of single-walled carbon nanotubes for an inhalation study. Inhalation Toxicology. 2008; 20:751–760. [PubMed: 18569097]

Chakravarty P, Marches R, Zimmerman NS, Swafford AD-E, Bajaj P, Musselman IH, Pantano P, Draper RK, Vitetta ES. Thermal ablation of tumor cells with antibody-functionalized single-walled carbon nanotubes. Proceedings of the National Academy of Sciences of the United States of America. 2008; 105(25):8697–8702. [PubMed: 18559847]

Clayton MP, Bancroft B, Rajan B. A review of assigned protection factors of various types and classes of respiratory protective equipment with reference to their measured breathing resistances. Annals of Occupational Hygiene. 2002; 46:537–547. [PubMed: 12176769]

Dahm M, Yencken M, Schubauer-Berigan M. Exposure control strategies in the carbonaceous nanomaterial industry. Journal of Occupational and Environmental Medicine. 2011; 53(6):S68–S73. [PubMed: 21654421]

Endo M, Strano MS, Ajayan PM. Potential applications of carbon nanotubes. Carbon Nanotubes. 2008; 111:13–61.

Han JH, Lee EJ, Lee JH, So KP, Lee YH, Bae GN, Lee S, Ji JH, Cho MH, Yu IJ. Monitoring multiwalled carbon nanotube exposure in carbon nanotube research facility. Inhalation Toxicology. 2008; 20:741–749. [PubMed: 18569096]

Howard, J., editor. [accessed 21.4.2005] Guidance for filtration an air-cleaning systems to protect building environments from airborne chemical, biological, or radiological attacks. 2003. Available from: ⟨http://www.cdc.gov/niosh/docs/2003-136/2003-136.html⟩

Khlystov A, Stanier C, Pandis SN. An algorithm for combining electrical mobility and aerodynamic size distributions data when measuring ambient aerosol. Aerosol Science and Technology. 2004; 38(Supplement 1):229–238.

Kim SC, Wang J, Emery M, Shin WG, Mullholand G, Pui DYH. Structural property effect of nanoparticle agglomerates on particle penetration through fibrous filter. Aerosol Science and Technology. 2009; 43(4):344–355.

Ku BK, Kulkarni P. Morphology of single-wall carbon nanotube aggregates generated by electrospray of aqueous suspensions. Journal of Nanoparticle Research. 2009; 11:1393–1403.

Maynard AD, Baron PA, Foley M, Shvedova AA, Kisin ER, Castranova V. Exposure to carbon nanotube material: aerosol release during the handling of unrefined single walled carbon nanotube material. Journal of Toxicology and Environmental Health A. 2004; 67(1):87–108.

Maynard AD, Ku BK, Emery M, Stolzenburg M, McMurry PH. Measuring particle size-dependent physiochemical structure in airborne single walled carbon nanotube agglomerates. Journal of Nanoparticle Research. 2007; 9:85–92.

McKinney W, Chen BT, Frazer D. Computer controlled multi-walled carbon nanotube inhalation exposure system. Inhalation Toxicology. 2009; 21:1053–1061. [PubMed: 19555230]

Mitchell L, Gao J, Vander Wal R, Gigliotti A, Burchiel S, McDonald J. Pulmonary and systemic immune response to inhaled multiwalled carbon nanotubes. Toxicology Science. 2007; 100:203–214.

Muller J, Huaux F, Moreau N, Misson P, Heilier JF, Delos M, Arras M, Fonseca A, Nagy JB, Lison D. Respiratory toxicity of multi-wall carbon nanotubes. Toxicology and Applied Pharmacology. 2005; 207:221–231. [PubMed: 16129115]

NIOSH (National Institute for Occupational Safety and Health). NIOSH current intelligence bulletin: occupational exposure to carbon nanotubes and nanofibers. 2010. Docket Number: (NIOSH-161A)Available from: ⟨http://www.cdc.gov/niosh/docket/review/docket161A/default.html⟩

Code of federal regulations title 42, Part 84. 1995. NIOSH-42 Part 84: Respiratory Protection Devices; p. 30335-30398.

Poland CA, Duffin R, Kinloch I, Maynard A, Wallace WA, Seaton A, Stone V, Brown S, Macnee W, Donaldson K. Carbon nanotubes introduced into the abdominal cavity of mice show asbestos-like pathogenicity in a pilot study. Nature Nanotechnology. 2008; 7:423–428.

Porter DW, Hubbs AF, Mercer RR, Wu N, Wolfarth MG, Sriram K, Leonard S, Battelli L, Schwegler-Berry D, Friend S, Andrew M, Chen BT, Tsuruoka S, Endo M, Castranova V. Mouse pulmonary dose- and time course-responses induced by exposure to multi-walled carbon nanotubes. Toxicologist. 2010; 269:136–147.

Rengasamy S, Eimer B, Shaffer RE. Comparison of nanoparticle filtration performance of NIOSH-approved and CE marked iltering facepiece respirators. Annals of Occupational Hygiene. 2009; 53(2):117–128. [PubMed: 19261695]

Rengasamy S, Miller A, Eimer B. Evaluation of the filtration performance of NIOSH-approved N95 filtering-facepiece respirators by photometric and number-based test methods. Journal of Occupational and Environmental Hygiene. 2011; 8:23–30. [PubMed: 21154105]

Rengasamy S, Verbofsky R, King WP, Shaffer RE. Nanoparticle penetration through NIOSH-approved N95 filtering-facepiece respirators. Journal of the International Society for Respiratory Protection. 2007; 24:49–59.

Seto T, Furukawa T, Otani Y, Uchida K, Endo S. Filtration of multi-walled carbon nanotube aerosol by fibrous filters. Aerosol Science and Technology. 2010; 44:734–740.

Shvedova AA, Kisin E, Murray AR, Johnson VJ, Gorelik O, Arepalli S, Hubbs AF, Mercer RR, Keohavong P, Sussman N, Jin J, Yin J, Stone S, Chen BT, Deye G, Maynard A, Castranova V, Baron PA, Kagan VE. Inhalation vs. aspiration of single-walled carbon nanotubes in C57BL/6 mice: inflammation, fibrosis, oxidative stress, and mutagenesis. American Journal of Physiology—Lung Cellular and Molecular Physiology. 2008; 295:L552–L565. [PubMed: 18658273]

Shvedova AA, Kisin ER, Mercer R, Murray AR, Johnson VJ, Potapovich AI, Tyurina YY, Gorelik O, Arepalli S, Schwegler-Berry D, Hubbs AF, Antonini J, Evans DE, Ku BK, Ramsey D, Maynard A, Kagan VE, Castranova V, Baron P. Unusual inflammatory and fibrogenic pulmonary responses to single walled carbon nanotubes in mice. American Journal of Physiology—Lung Cellular and Molecular Physiology. 2005; 289:L698–L708. [PubMed: 15951334]

Vo E, Shaffer R. Development and characterization of a new test system to challenge personal protective equipment with virus-containing particles. Journal of the International Society for Respiratory Protection. 2012; 29:13–29.

Wang J, Kim SC, Pui DYH. Measurement of multi-wall carbon nanotube penetration through a screen filter and single-fiber analysis. Journal of Nanoparticle Research. 2011a; 45:443–452.

Wang J, Kim SC, Pui DYH. Carbon nanotube penetration through a screen filter: numerical modeling and comparison with experiments. Aerosol Science and Technology. 2011b; 45:443–452.

Wang J, Pui DYH. Numerical investigation of filtration by fibers with elliptical cross-sections. Journal of Nanoparticles Research. 2009; 11(1):185–196.

Wilkes AR. Comparison of two techniques for measuring penetration of sodium chloride particles through breathing system filters. British Journal of Anaesthesia. 2002; 89:541–545. [PubMed: 12393352]

World Technology Evaluation Center (WTEC). [accessed 12.12.2010] WTEC panel report on international assessment of research and development of carbon nanotube manufacturing and applications. 2007. Available from: ⟨http://www.wtec.org/cnm/CNM_final_report.pdf⟩

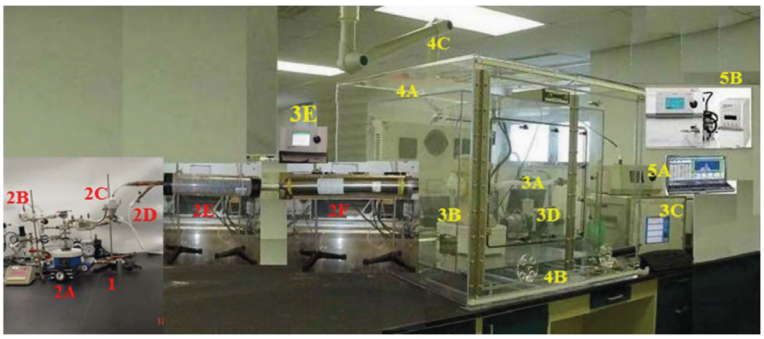

Fig. 1.

CNT-ARTS: air supply with HEPA filters (1); CNT aerosol generator (2A); air inlet (2B); cyclone (2C); dilution air (2D); diffusion dryer (2E); neutralizer (2F); exposure chamber (3A); head form (3B); breathing simulator (3C); exhaust port (3D); CPC (3E); secondary containment (4A); ventilation air inlet (4B); ventilation air outlet (4C); APS (5A); SMPS (5B).

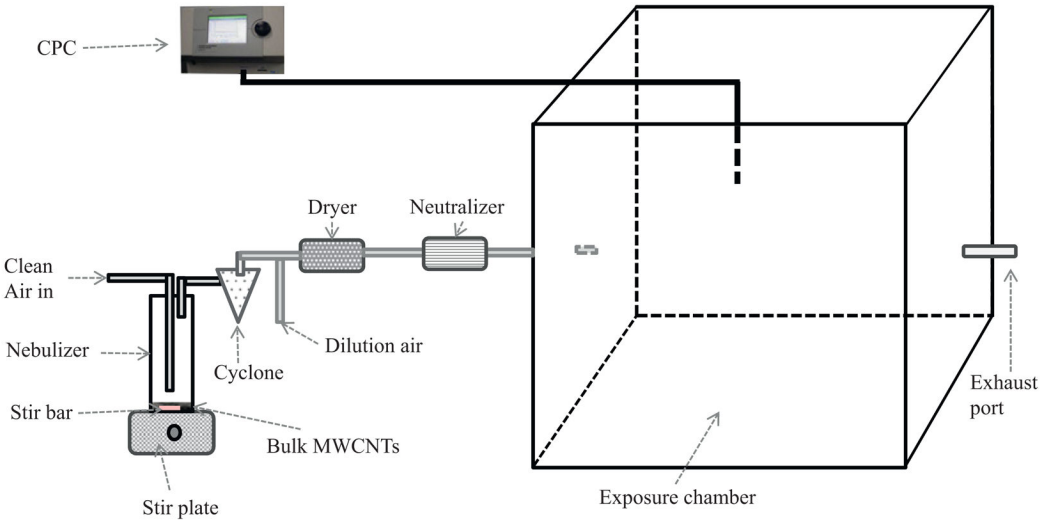

Fig. 2.
CNT aerosol generation system.

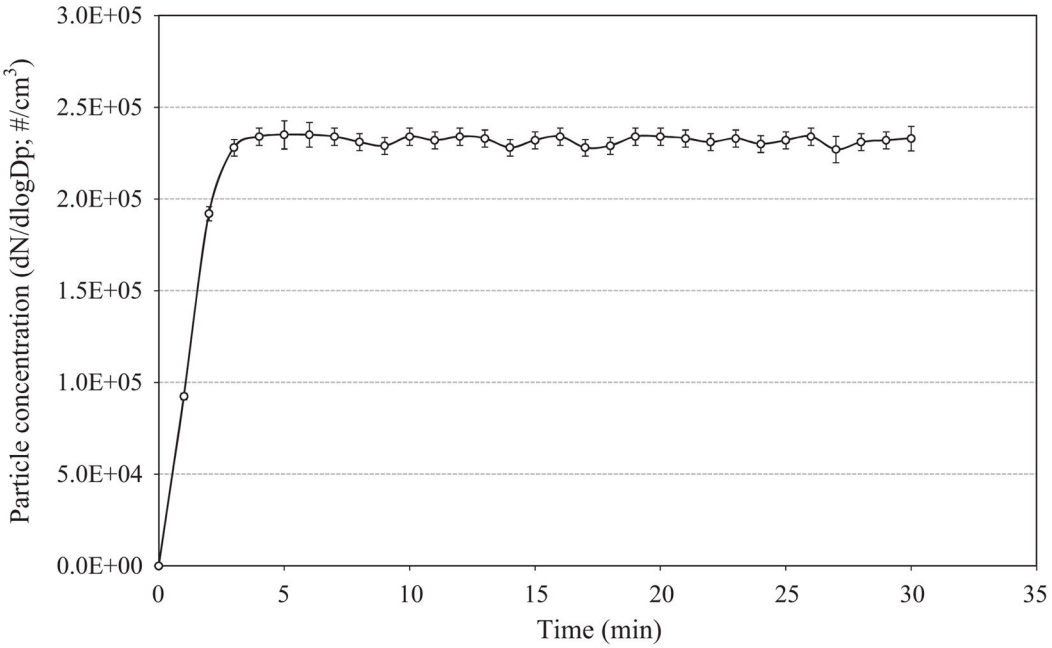

Fig. 3.

Average MWCNT concentration (*n*=3) at the center of the exposure chamber during a 30-minute test period.

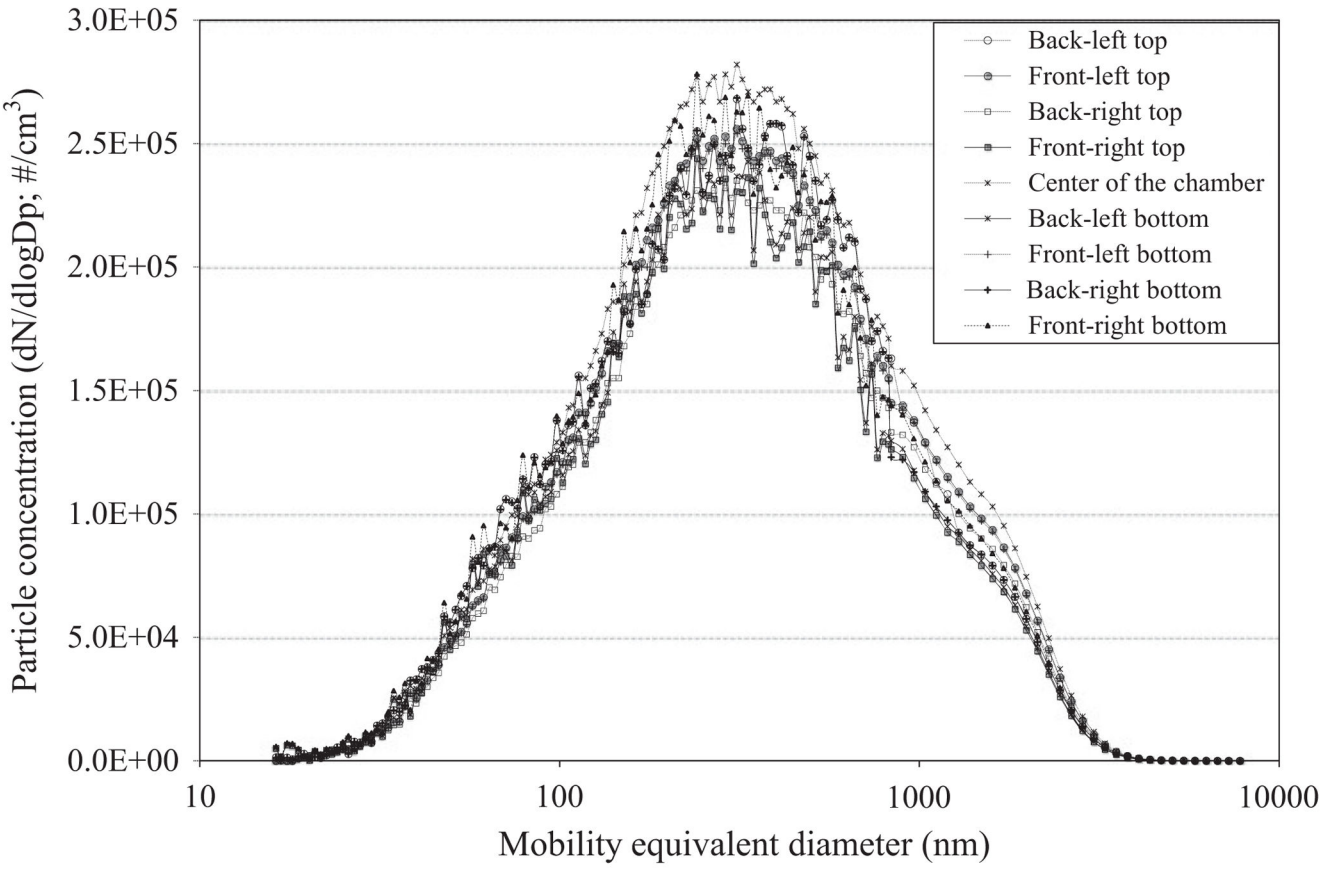

Fig. 4.

Size distribution of the airborne MWCNTs at different chamber locations measured using the SMPS and APS.

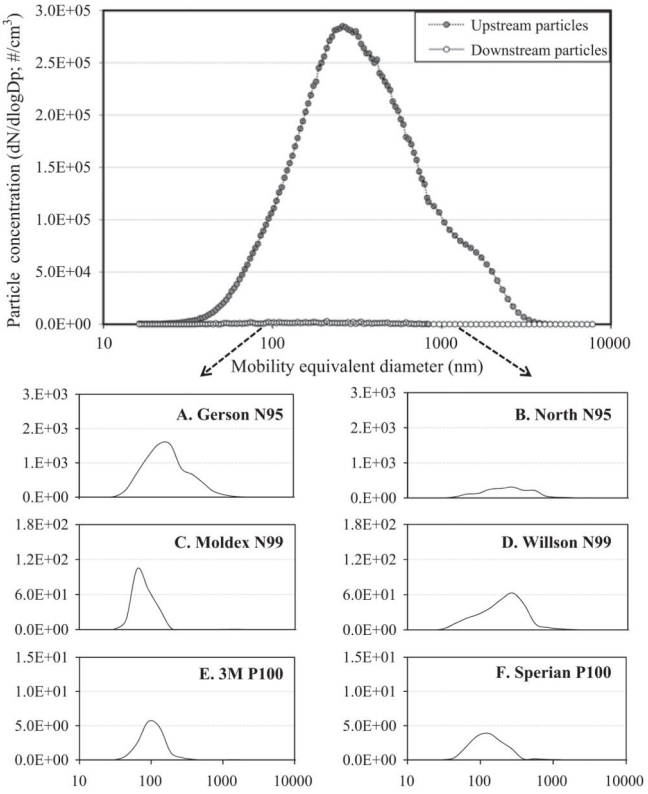

Fig. 5.

Size distribution of upstream and downstream MWCNTs at the 30-LPM flow rate measured using the SMPS and APS (A–F: downstream MWCNTs; *n*=3 for each model).

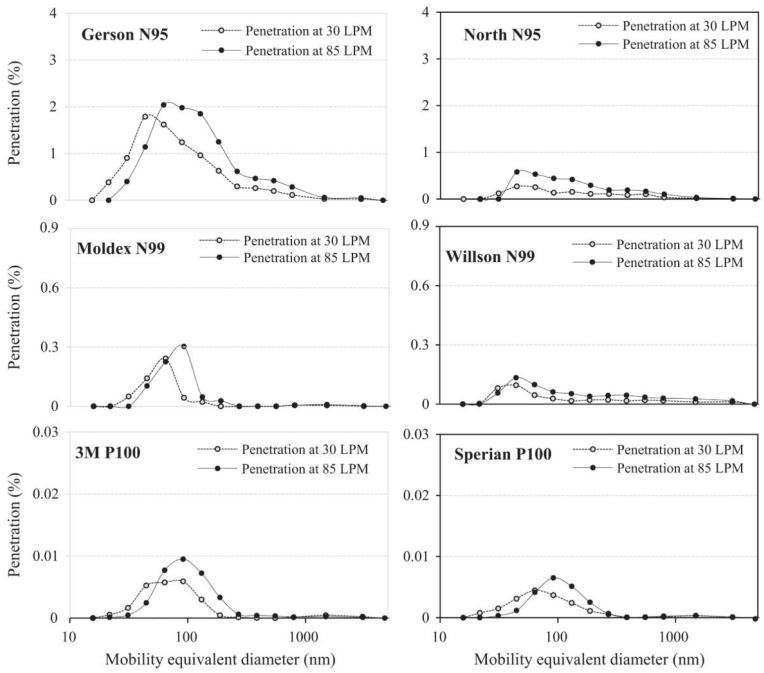

Fig. 6.

Mean MWCNT penetration (count penetration; *n*=3 for each model at each flow rate) through the tested FFRs as a function of individual particle size measured using APS and SMPS.

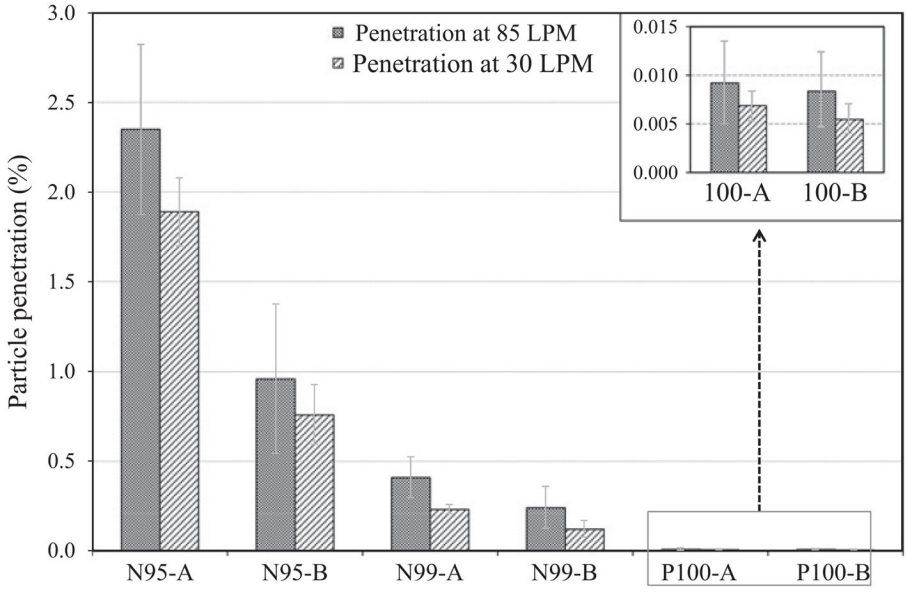

Fig. 7.

Total MWCNT penetration of all particle sizes through the tested FFRs at the flow rates of 30 and 85 LPM (*n*=3 for each FFR at each flow rate): N95-A: Gerson N95; N95-B: North N95; N99-A: Moldex N99; N99-B: Willson N99; P100-A: 3M P100; P100-B: Sperian P100.

Table 1

FFRs used in the penetration study.

FFR series	FFR models	FFR information
N95	Gerson 1730	Manufacturer: www.GersonCo.com Middleboro, MA 1-800-225-8623
	North 7130	Manufacturer: www.northsafety.com Cranston, RI 02921 1-800-430-4110
N99	Moldex 2310	Manufacturer: www.moldex.com Culver City, CA 90232 1-310-837-6500
	Willson N1139 M/L	Manufacturer: Willson Santa Ana, CA 92704 1-800-821-7236
P100	3M 8293	3M Canada Company P.O. Box 5757 London, Ontario N6A 4T1 1-651-737-6501
	Sperian P1130S	Retail: www.drillspot.com 1-720-204-3660